BACHELOR

Creating a 3D Model with a Controlled Surface Roughness

van Wanrooij, Chiel A.J.

Award date:
2023

Department of Mechanical Engineering

2022-2023 quartile 1 & 2

Creating a 3D Model with a Controlled Surface Roughness

Bachelor End Project

Eindhoven, January 24, 2023

Project coordinators:
G.J. Wensink
M. Rücker

Authors:
C.A.J. van Wanrooij

Contents

1 Introduction

Among the principal challenges of the twenty-first century are how to secure access to clean water for drinking and agriculture, and how to provide sufficient energy for a growing and hopefully more prosperous population, while coping with the threat of climate change. The economics and social aspects of these challenges have a common scientific underpinning: flow in porous media. The majority of the world's freshwater resides underground in aquifers; most of our energy comes from oil and gas extracted from porous rock; and one promising method to reduce atmospheric emissions of carbon dioxide is to collect it from major sources, such as fossil-fuel burning power stations, and inject it deep underground into saline aquifers or depleted hydrocarbon reservoirs. Indeed, global-scale carbon dioxide storage is necessary if we are to avoid dangerous climate change. In any event, the understanding and management of fresh water, oil and gas recovery and carbon dioxide storage all rely on quantifying how fluids flow through porous rocks.[1]

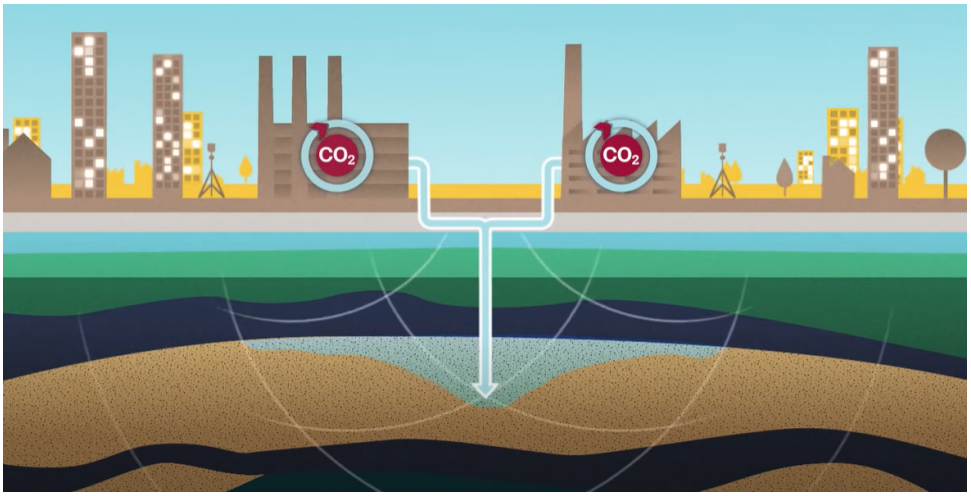

Figure 1.1: CO2 storage in porous media[2]

Surface roughness can affect multiphase flow in porous media in several ways. It can increase the resistance to flow, which can lead to a decrease in the flow rate. It can also alter the distribution of the different phases within the porous media, as roughness can cause one phase to preferentially flow through certain areas while the other phase flows through other areas.[3]

In order to comprehend the relationship between surface roughness and fluid displacement, it is essential to consider the way in which a liquid interacts with a solid surface. The interaction of a liquid with a solid is characterized by the word 'Wetting'. It can be the spreading of a liquid over a solid surface, the penetration of a liquid into porous materials, or the displacement of one liquid by another. This phenomenon can help to characterize a surface, and to determine the interaction, between a solid and a liquid. One way to quantify a liquid's surface wetting characteristics is to measure the contact angle of a drop of liquid placed on the surface of an object. The contact angle is the angle formed by the solid/liquid interface and the liquid/vapor interface measured from the side of the liquid. Liquids wet surfaces when the contact angle is less than 90°. For a penetrant material to be effective, the contact angle should be as small as possible. In fact, the contact angle for most liquid penetrants is very close to 0°.[4]

The Cassie-Baxter state is characterized by the liquid droplets being supported by the solid surface's roughness, resulting in a reduced contact area between the liquid and solid. This leads to an increased apparent superhydrophobicity. On the other hand, the Wenzel state occurs when the liquid droplets fill in the surface roughness and make contact with the solid surface. This results in an increased contact area between the liquid and solid. This state is often referred to as "complete wetting".[5]

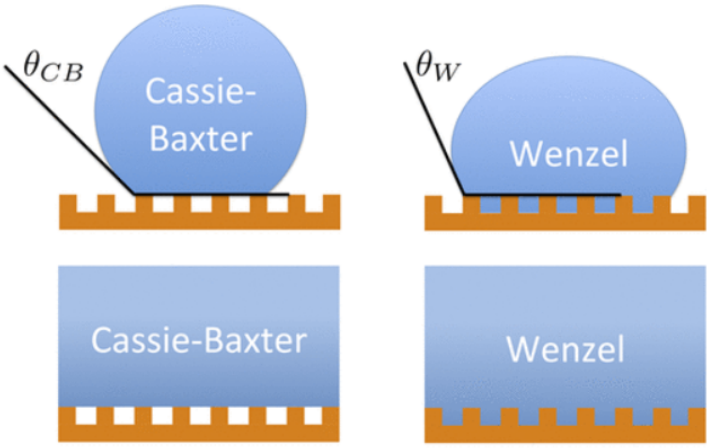

Figure 1.2: Cassie-Baxter and Wenzel[5]

We want to systematically investigate the relation between surface structure and multiphase flow dynamics, hence we search for a systematic method to vary this property. Natural surface roughness can be recreated by artificial structures. There are several known methods of recreating surface roughness:[6][7]

- Mechanical methods: These involve using abrasive tools or machines to create roughness on the surface. Examples include sandblasting, grinding, and machining.
- Chemical methods: These involve using chemicals to etch or corrode the surface to create roughness. Examples include acid etching and anodization.
- Electrolytic methods: These involve using an electrical current to create roughness on the surface. Examples include electrolytic grinding and electrochemical machining.
- Physical methods: These involve using physical processes, such as frosting or irradiation, to create roughness on the surface.
- Thermal methods: These involve using heat to alter the surface of the material, creating roughness. Examples include flame spraying and thermal oxidation.
- Laser methods: These involve using a laser to create roughness on the surface. Examples include laser ablation and laser texturing.

In this research both mechanical and chemical methods are used to roughen the surface. The goal is to quantify the surface roughness with several roughness parameters for different methods, to finally creating a 3D-model with a controlled surface roughness.

2 Roughness parameters

Roughness parameters are used in a wide variety of applications, including:[8]

- Manufacturing: In manufacturing, roughness parameters are often used to describe the surface finish of machined or molded parts. The roughness of a surface can affect how the part functions, and roughness parameters are used to ensure that parts meet specified surface finish requirements.
- Tribology: In tribology (the study of friction, wear, and lubrication), roughness parameters are used to describe the roughness of surfaces that are in contact with each other. The roughness of a surface can affect the friction and wear characteristics of the surface, and roughness parameters are used to understand and optimize these characteristics.
- Aerospace: In the aerospace industry, roughness parameters are used to describe the roughness of aircraft surfaces, such as wing and fuselage surfaces. The roughness of these surfaces can affect the aerodynamic performance of the aircraft, and roughness parameters are used to ensure that the surfaces meet specified roughness requirements.
- Medical devices: In the medical industry, roughness parameters are used to describe the roughness of medical devices, such as implants and catheters. The roughness of these devices can affect how they function and interact with the body, and roughness parameters are used to ensure that the devices meet specified roughness requirements.
- Food processing: In the food industry, roughness parameters are used to describe the roughness of surfaces that come into contact with food, such as conveyor belts and packaging materials. The roughness of these surfaces can affect how the food is processed and handled, and roughness parameters are used to ensure that the surfaces meet specified roughness requirements.

The parameters can be characterised in the amplitude parameters, the spacing parameters and the hybrid parameters. The parameters that are relevant for this research will be explained a bit further.[9]

2.1 The amplitude parameters

Amplitude parameters are the most important parameters to characterise surface topography. They are used to measure the vertical characteristics of the surface deviation. The vertical characteristics of surface roughness and flow in porous media can have a significant impact on the overall fluid flow through the media. In general, surface roughness can increase the resistance to fluid flow through the media. This is because the roughness creates additional surface area for the fluid to flow over[10], which increases the viscous forces acting on the fluid. The roughness can also create channels or valleys that the fluid can flow through, which can affect the flow patterns and the overall resistance to flow. The vertical characteristics of the roughness, such as the height and distribution of the roughness features, can also affect the fluid flow. The increase in surface area can increase the fluid's resistance to flow, conversely, the fluid's wetting state can decrease the fluid's resistance to flow. This section will provide a brief description of the relevant amplitude parameters.

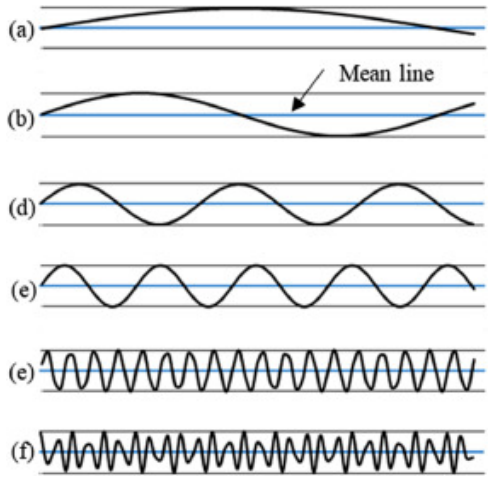

Figure 2.1: Additional surface area

2.1.1 Arithmetic Average Height (R_a)

The arithmetic average height parameter is the most universally used roughness parameter for general quality control. It is often used to ensure that the surface finish of a product meets specified roughness requirements. It is a simple and straightforward measure of roughness that is easy to calculate, and is therefore widely used in manufacturing and quality control. It is defined as the average absolute deviation of the roughness irregularities from the mean line over one sampling length. This parameter is easy to define, easy to measure and gives a good general description of height variations. It does not give any information about the wavelength and it is not sensitive to small changes in profile. The mathematical definition of the arithmetic average height parameter is as follow:[9]

$$R_a = \frac{1}{l} \int_0^l |y(x)| \, dx \tag{2.1}$$

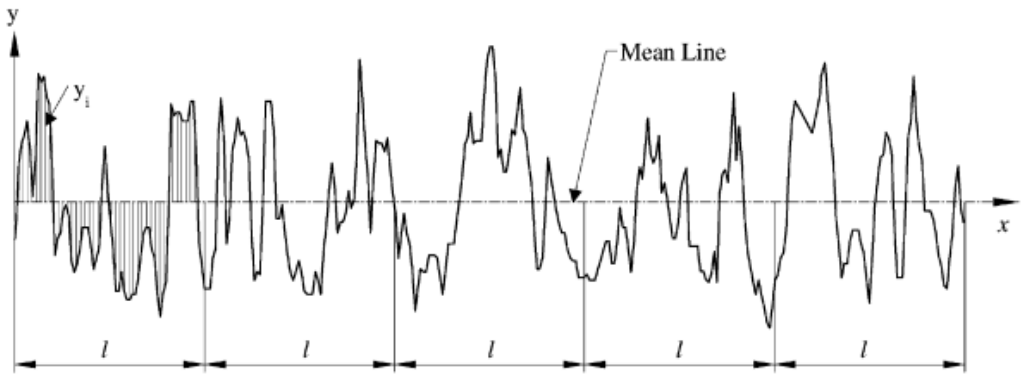

Figure 2.2: Arithmetic Average Height

The roughness Ra has an obvious impact on the wetting state of water droplet. With the increase of Ra, the water droplet is converted from Wenzel state to Cassie state.[11]

2.1.2 Root Mean Square Roughness (R_q)

This parameter represents the standard deviation of the distribution of surface heights, so it is an important parameter to describe the surface roughness by statistical methods. This parameter is more sensitive than the arithmetic average height to large deviation from the mean line. The mathematical definition of this parameter is as follow:[9]

$$R_q = \sqrt{\frac{1}{l} \int_0^l y(x)^2 \, dx} \tag{2.2}$$

2.1.3 Maximum peak to valley height (PV)

The peak to valley height is the vertical distance between the highest peak an d the lowest valley for each sampling length of the profile.[9]

2.2 The spacing parameters

The spacing parameters are those which measure the horizontal characteristics of the surface deviations. The spacing parameters are important for wettability of the surface.[9] With the increase of the pillar spacing, the droplet contact angle gradually decreases. When the spacing is large enough, the droplet can enter the gap closest to the droplet and completely fill the gap. [11]

2.2.1 Mean spacing at mean line (S_m)

This parameter is defined as the mean spacing between profile peaks at the mean line. The profile peak is the highest point of the profile between upwards and downwards crossing the mean line. The

mathematical definition of this parameter is as follow:

$$S_m = \frac{1}{N}\sum_{i=1}^{n} S_i \tag{2.3}$$

Where N is the number of profile peaks at the mean line. S_m is measured at the intersection of the profile with the mean line.[9]

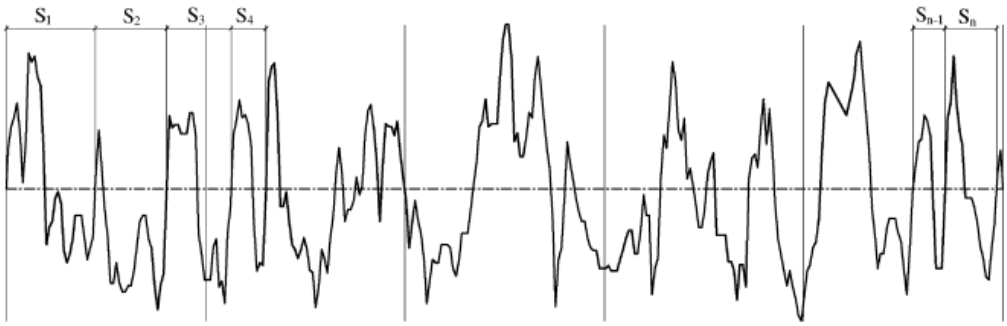

Figure 2.3: mean spacing at mean line

2.2.2 Peak count (P_c)

The peak count parameter is defined as the number of local peaks, which is projected through a selectable band located above and below the mean line by the same distance. The number of peak count is determined along the assessment length and the result is give in peaks per millimetre. The peak count is determined only for the closed areas of the profile, in which the profile intersects each the upper and the lower bands in two points at least.[9]

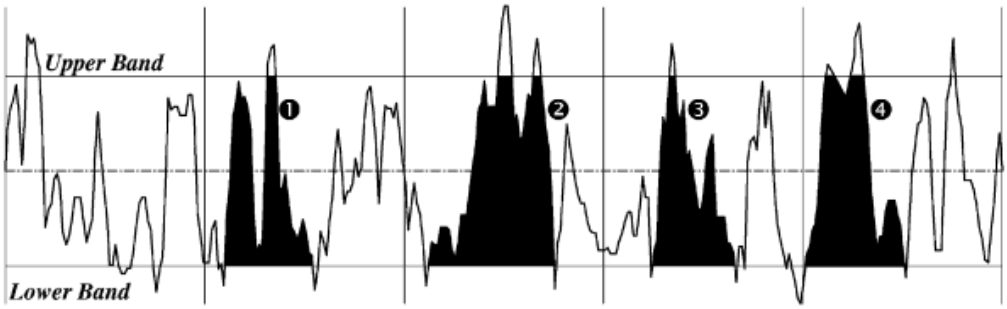

Figure 2.4: Peak count

2.3 The hybrid parameters

The hybrid property is a combination of amplitude and spacing. Any changes, which occur in either amplitude or spacing, may have effects on the hybrid property. In tribology analysis, surface slope, surface curvature and developed interfacial area are considered to be important factors, which influence the tribological properties of surfaces.[9]

2.3.1 Mean slope of the profile (Δ_a)

This parameter is defined as the mean absolute profile slope over the assessment length. This parameter can be calculated by calculating all slopes between each two successive points of the profile. then calculating the average of these slopes. The mathematical definition is as follow:[9]

$$\Delta_a = \frac{1}{L}\int_0^L |\frac{dy}{dx}|\, dx \tag{2.4}$$

3 Experiment

3.1 Etching with acid

3.1.1 Method

In this experiment a chemical mixture will be considered to modify the surface roughness of stainless steel spheres and glass beads, with both a diameter of 3 millimeter. This chemical mixture consist of nitric acid and hydrofluoric acid and the industrial naming is Pelox SP-K 3000 mixture. The unmodified samples will be taken as reference. A few samples will be modified with the chemical mixture and the duration of exposure will vary. All samples that are exposed to the acid, are washed with dasty and distilled water to neutralize the acid. For the modification of the stainless steel spheres, the following materials are used:

- *Pelox SP-K 3000
- *Dasty
- distilled water
- 3mm stainless steel spheres
- 3mm glass beads

*Pelox SP-K 3000 is a mixture that consists of nitric acid and hydrofluoric acid.
*Dasty is a mixture that consists of among other things ethanolamine and potassium phosphate.

3.2 Sandblasting

3.2.1 Method

In this experiment sandblasting with glass is considered. The glass parts with a diameter of 20 micron are shot at the sample surfaces. With the blastingcabin it is possible to safely sandblast with a working pressure of 3 to 6 bar. At a full pressure of 6 bar, you use approximately 250 liters of blasting glass per minute. To make sure that the samples were held in place, a metal mesh was used. However, this still did not prevent the samples from spinning. Due to this spinning, the surface of the samples could not be modified consistent over the whole sample.

3.3 Grinding with sandpaper

3.3.1 Method

The last method that is considered is grinding the samples with sandpaper. The first sandpaper is attached to a table, so that it won't move. A second sandpaper is used on top of the first sandpaper with the samples in between the two sandpapers. A considerable consistent pressure is applied on the samples. As well as a circular motion to make sure that most of the surface will be modified. The following grainsizes are used:

- P4000, with a grain size of 5 micrometer
- P2400, with a grain size of 8 micrometer
- P2000, with a grain size of 10 micrometer

4 Measurements

To measure the topography of the modified samples, two different methods are used. The first one is the atomic force microscope and the second is a confocal surface profilometer.

4.1 Atomic Force Microscope

The AFM is a high-resolution non-optical imaging technique. This is used to measure properties of a surface on atomic scale, such as the topography.

4.1.1 Working principle

The basic operation principle of a standard AFM system with optical feedback involves scanning an AFM probe with a sharp AFM tip over a sample surface in a raster pattern. The AFM tip is usually made of silicon or silicon nitride and is integrated near the free end of a flexible AFM cantilever. A piezoelectric ceramic scanner controls the lateral and the vertical position of the AFM probe relative to the surface. In contact mode, as the AFM tip moves over features of different height the deflection of the AFM cantilever changes. This deflection is tracked by a laser beam reflected from the back side of the AFM cantilever and directed into a position sensitive photodetector. A feedback loop controls the vertical extension of the scanner in order to maintain near-constant AFM cantilever deflection and hence a constant interaction force. The coordinates that the AFM tip tracks during the scan are combined to generate a three-dimensional topographic image of the surface.[12]

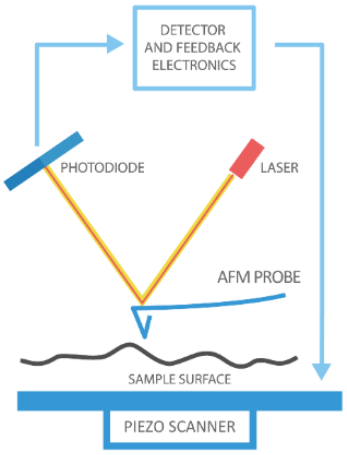

Figure 4.1: AFM schematic[13]

The quantitative imaging (QI) mode of AFM is a multiparametric imaging mode that collects not only topographical information but also quantitative information on the mechanical properties of the sample surface. This is achieved by measuring force-distance curves at every pixel in a high resolution image, as opposed to the traditional method which requires two separate measurements for high resolution topography and low resolution force mapping. The force-distance curve is a plot of the force experienced by the probe as it approaches and retracts from the sample surface. The curve typically has two regions: an attractive region, where the force is negative and the probe is pulled towards the sample, and a repulsive region, where the force is positive and the probe is pushed away from the sample. By analyzing the shape and parameters of the force-distance curve, it is possible to extract information on the height, surface stiffness and adhesion of the sample surface at each high resolution pixel. This multiparametric information can be used to gain a deeper understanding of the sample surface and its properties. For example, the adhesion force can be used to infer the chemical nature of the sample surface, while the surface stiffness can be used to infer its mechanical properties. Additionally, by combining topographical and mechanical information, it is possible to create detailed 3D maps of the sample surface, highlighting different regions with different mechanical properties. Overall, the QI mode of AFM is a powerful tool for high resolution imaging and characterization of samples, with the ability to provide detailed information on the sample surface in a single measurement.[14]

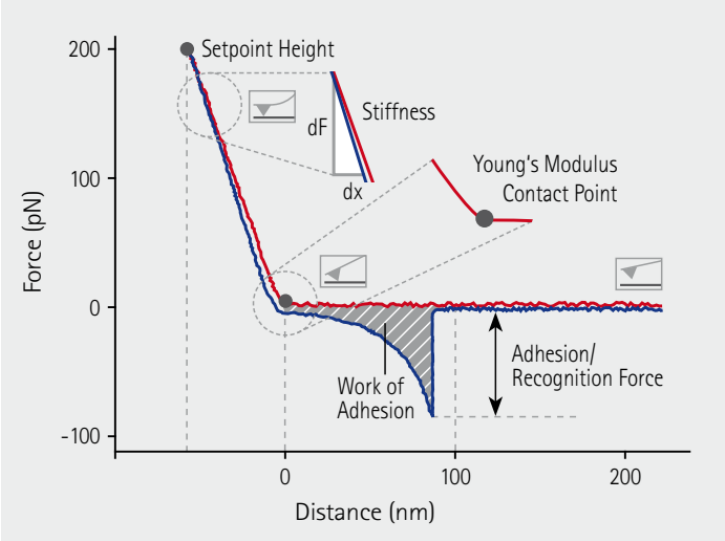

Figure 4.2: QI mode[14]

4.2 Confocal Surface Profilometer

4.2.1 Working principle

Confocal technology is able to measure the surface height converting conventional images into optical sections where the signal is preserved for those areas within the depth of focus of the objective, improving the image contrast and the lateral resolution and system noise.[15] A light source travels through a pinhole and a lens when the light source is split in two. As can be seen in Figure 4.3. The light travels then through the chosen objective and with the Z-motor the focus on the sample will change. All these layers on top of each other will create a three-dimensional topographic image of the surface. One of the key features of a confocal surface profilometer is its ability to measure the surface topography with high lateral resolution and depth sensitivity. The lateral resolution is determined by the size of the pinhole and the wavelength of the laser, while the depth sensitivity is determined by the size of the laser focus and the numerical aperture of the collection optics. Confocal surface profilometers can achieve lateral resolutions on the order of a few micrometers and depth sensitivities on the order of a few nanometers.

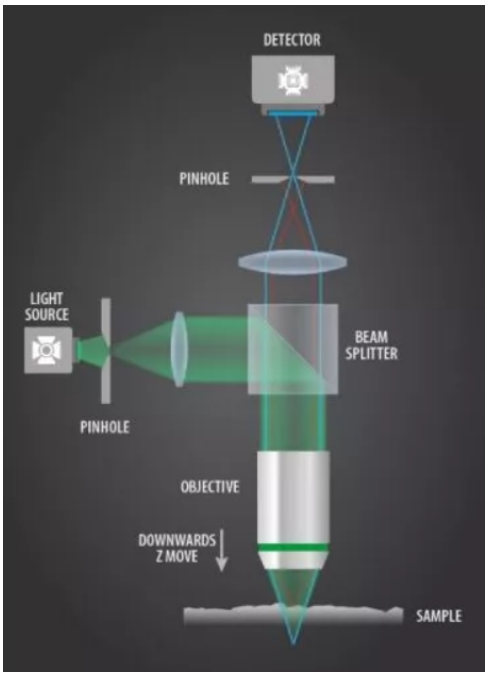

Figure 4.3: Confocal surface profilometer principle[15]

5 Analysis

5.1 Software

The analysis will be done with data processing software. The data processing of the AFM is done with the JPKSPM data processing software. The data processing of the confocal surface profilometer is done with the Plu 2.41 software. In this software, the data received from the AFM and the confocal surface profilometer can be analysed by using several surface roughness parameters, such as the arithmetic average height and the mean spacing at mean line. Both the software used for processing the data collected from the AFM as from the confocal surface profilometer work likewise. The software provides some filters, such as a plane/sphere fit. This filters out the curvature of the sample. Both software provides relevant roughness parameters. Matlab is eventually used to group all the data in visible figures to find any relevant correlations. In the next section the results from the collected data will be presented.

5.2 Interpolation NaN-values

The NaN-values in the collected data are interpolated with the inplaint-nans function in matlab. The method to interpolate the missing values uses a spring metaphor. It assumes springs with a nominal length of zero and connect each node with every neighbor (horizontally, vertically and diagonally). Since each node tries to be like its neighbors, extrapolation is as a constant function where this is consistent with the neighboring nodes.

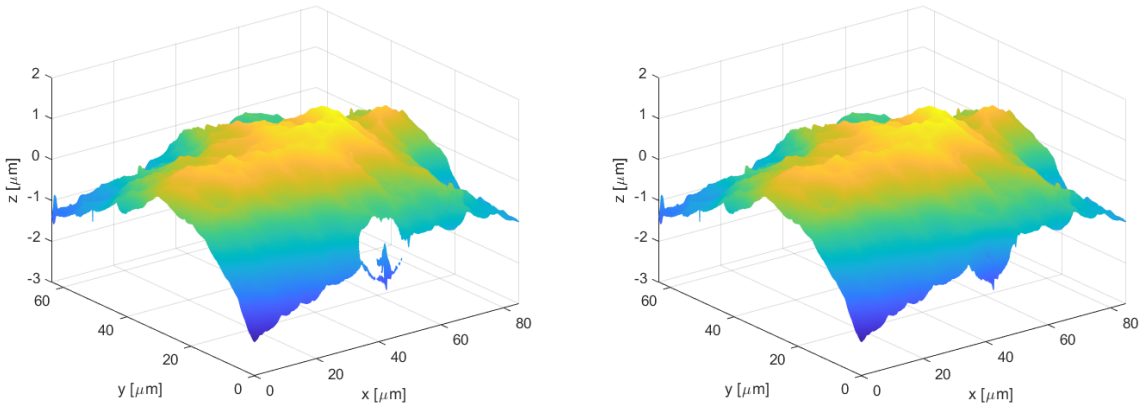

Figure 5.1: Interpolation surface area

5.3 Plane fit data

A spherical surface with known origin and radius is created. These parameters are known due to measurements on the considered sample. The location of the points on the created spherical surface are subtracted from the data points of the confocal profilometer. This gives a plane-like view of the confocal profilometer data at a distance equal to the radius of the created sphere. The x and y needs to be the same size, so a meshgrid is used. The following equation is used for the plane fit:

$$Z_{plane} = Z_1 - \sqrt{r^2 - (X_1 - X_0)^2 - (Y_1 - Y_0)^2} - Z_0 \tag{5.1}$$

Where, Z_1 is the measured interpolated z-coordinates in a matrix, r is the radius of the created sphere, X_1 is the measured x-coordinates, X_0 is the x-coordinate of the origin of the created sphere, Y_1 is the measured y-coordinates, Y_0 is the y-coordinate of the origin of the created sphere, Z_0 is the z-coordinate of the origin of the created sphere.

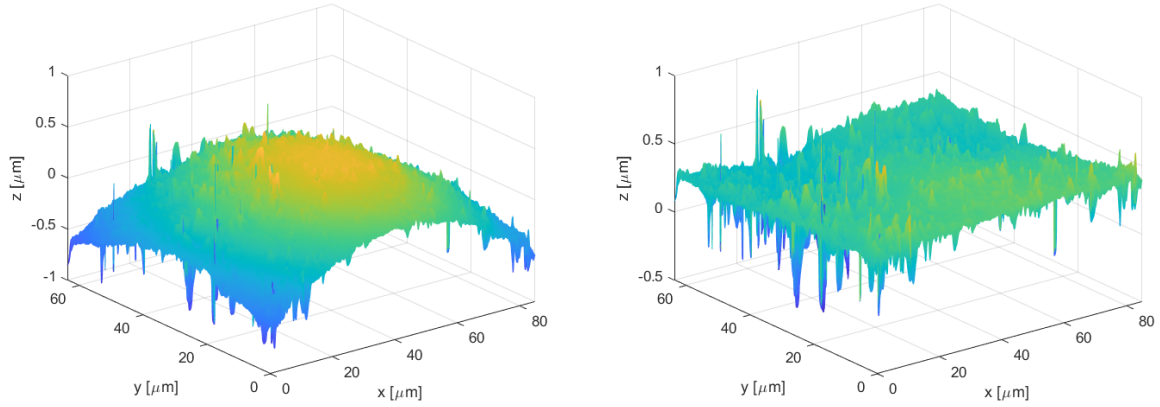

Figure 5.2: Plane fit surface area

5.4 Boxplot

A box plot uses boxes and lines to depict the distributions of one or more groups of numeric data. Box limits indicate the range of the central 50 percent of the data, with a central line marking the median value. Lines extend from each box to capture the range of the remaining data, with dots placed past the line edges to indicate outliers.[16]

Construction of a box plot is based around a dataset's quartiles, or the values that divide the dataset into equal fourths. The first quartile (Q1) is greater than 25 percent of the data and less than the other 75 percent. The second quartile (Q2) sits in the middle, dividing the data in half. Q2 is also known as the median. The third quartile (Q3) is larger than 75 percent of the data, and smaller than the remaining 25 percent. In a box and whiskers plot, the ends of the box and its center line mark the locations of these three quartiles.[16]

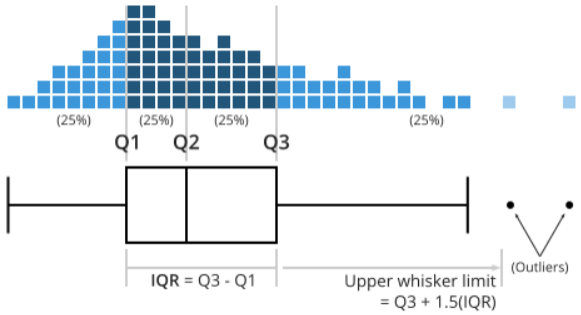

Figure 5.3: boxplot[16]

The distance between Q3 and Q1 is known as the interquartile range (IQR) and plays a major part in how long the whiskers extending from the box are. Each whisker extends to the furthest data point in each wing that is within 1.5 times the IQR. Any data point further than that distance is considered an outlier, and is marked with a dot.[16]

6 Results - AFM

6.1 AFM - Glassbeads etching with acid

In the following figures the etching of glass with acid is shown. In Figure 6.1a an unmodified glassbead is shown. In Figure 6.1b a modified glassbead in HF for 45 minutes is shown. the left figure has an area of 10x10 μm^2, the right figure has an area of 40x40 μm^2

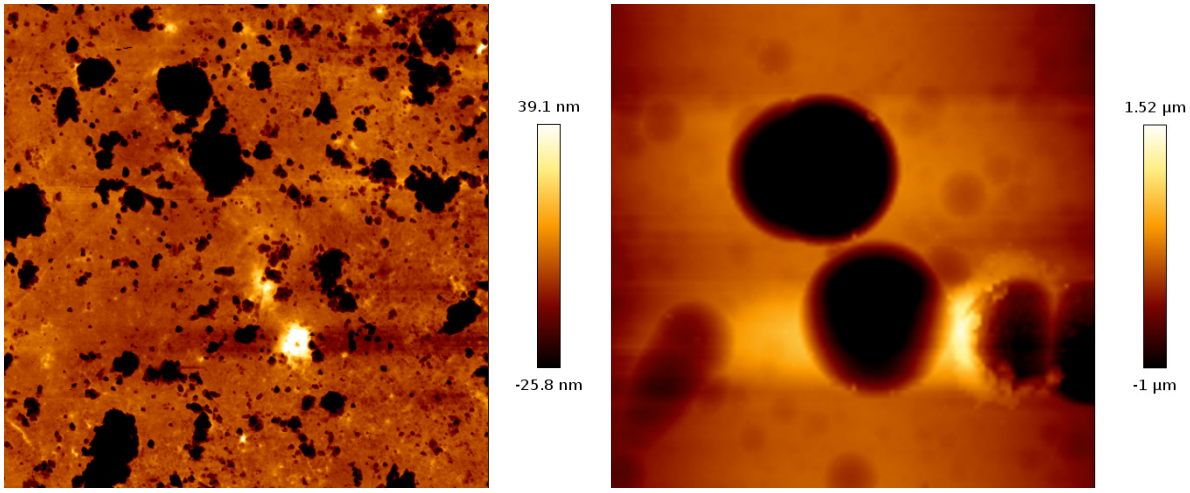

(a) no modification

(b) 45min HF modification

Figure 6.1: JPK image

The surface that is unmodified is considered as reference surface. The surface is relatively smooth. However, there are some small inequalities on the surface. A surface is not atomically flat because atoms are not arranged in perfectly regular patterns on a surface. The positions of atoms on a surface are influenced by factors such as the presence of impurities or defects.[17] In Figure 6.1a it can be seen that the shapes of the inequalities are random. After 45 minutes of HF modification on the glassbeads surface it becomes much rougher. The inequalities by magnitude in the surface become larger, but the shape of it becomes more predictable. The shapes of the big craters are almost perfectly circular. In the table below the different roughness parameters are specified on a line element of the same size. The line on the reference surface is randomly chosen, while the line on the modified surface is positioned on a part that exclude the big craters. This is done to show there is not only difference in surface roughness close around the craters. The parts that seem relatively smooth in Figure 6.1b have actually much higher values for the roughness parameters.

Roughness parameters	Average Roughness [nm]	RMS Roughness [nm]	Peak-to-Valley Roughness [nm]
Reference Surface	6.28	8.72	64.90
Surface HF modification	63.98	73.34	252.00

7 Results - Confocal surface profilometer

Most of the data that is collected is done with the confocal surface profilometer. Three objectives are used: the '20x objective', the '50x objective' and the '150x objective'. The 20x and 50x objective did not satisfy the requirements of this research. The Δx and Δy per pixel for the 20x and 50x objectives were 830 nanometer and 332 nanometer, respectively. The 150x objective was the best option. it had 768 data points on the x-axis and 576 data points on the y-axis. The Δx and Δy per pixel is 110.6 nanometer. The data that is collected with the 20x and 50x is in a table that can be found in the appendix. The data from the 150x is discussed further is this research.

7.1 Surface area

7.1.1 Calculation mathematically smooth surface

The change in surface area is a good indication of the surface roughness over the whole surface. Where some roughness parameters only give an indication over one sample line. The change in surface area is a combination of the roughness parameters. The area was not just a regular sphere-cap. So, the area of a mathematically perfectly smooth surface needed to be calculated with the use of NX12. A rectangle of 84.83x63.60 μm^2 is drawn. Subsequently, an arc with a radius of 1.5 μm was drawn between each point on the rectangle, with each arc being oriented at 90 degrees to the plane of the rectangle. A plane was subsequently constructed between these arcs, resulting in an area that was identical to the area of the quadrilateral as measured by a confocal profilometer. The area of the smooth surface is 5.3963e^3 μm^2

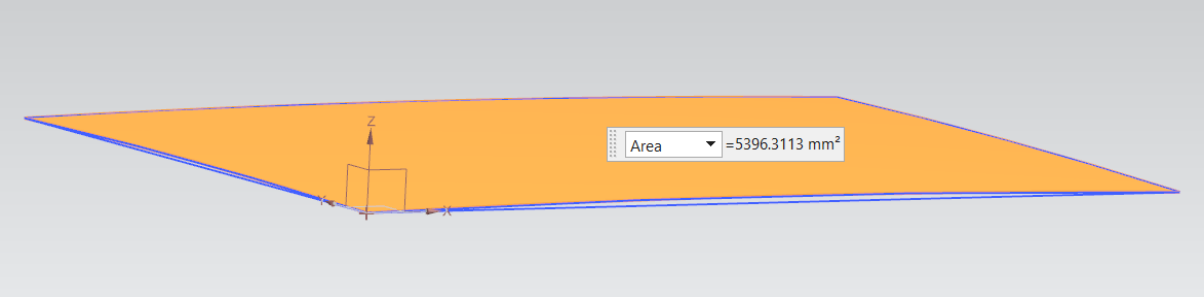

Figure 7.1: mathematically perfectly smooth surface area

7.1.2 Increase surface area of different modifying methods

In order to ensure the reliability of the data presented in the box charts, multiple samples were measured for each box. Specifically, for every box in the box charts, four different samples were measured.

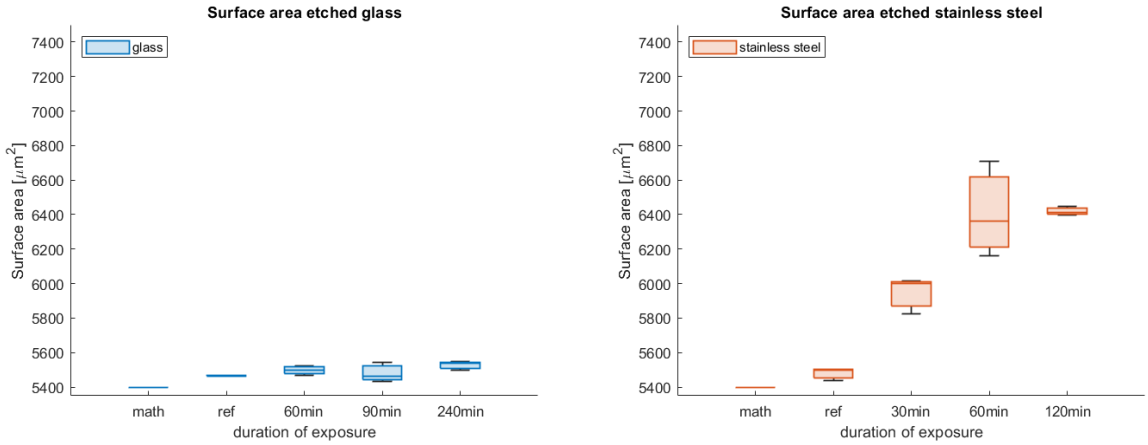

Figure 7.2: Surface area etched samples

In Figure 7.2 the surface areas of modified samples are presented. The "math" box represents the surface area when a mathematical quadrilateral is considered, while the "ref" box represents the unmodified samples. The other boxes correspond to the modified samples. It is observed that the increase in surface area for the glass beads is negligible. However, the acid etching process results in the formation of large, smooth, circular craters on the surface, which do not significantly contribute to the increase in surface area. In contrast, the increase in surface area for the stainless steel spheres is considerably greater. The surface profile of stainless steel remains more consistent relative to glass, but the size of the peaks and valleys more than double, thereby increasing the overall surface area.

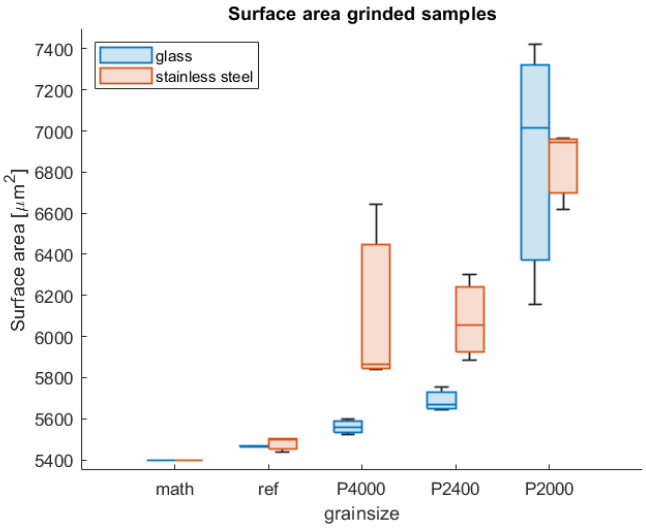

Figure 7.3: Surface area grinded samples with sandpaper

The surface area of a given material can be affected by various factors, including the size of the abrasive particles used in the process of surface modification. Specifically, it has been observed that when larger grain sizes are utilized for both glass beads and stainless steel spheres, the resulting surface area increases. This phenomenon can be attributed to the increased ability of larger abrasive particles to reach and abrade more surface area, leading to a greater overall surface roughness. The spreading of the data for glass at P4000 and P2400 is quite small. In contrast, the spreading of the data for glass at P2000 is significantly larger. The spreading for stainless steel is for all the three grainsizes more or less the same.

7.2 Connectivity

7.2.1 Mean curvatures

The mean curvature is a scalar measure of curvature, is defined as the average of the two principal curvatures, it can be written as (k1+k2)/2 where k1 and k2 are the two principal curvatures.[18] The mean curvature is a way to measure how much the surface deviates from being a plane, it can give information of how much the surface bend in some direction. The mean curvature of a surface is a key parameter in understanding the behavior of fluid flow over the surface. In order to visualize the impact of mean curvature on fluid flow, it is useful to consider the shape of the surface with positive and negative values of mean curvature. As shown in Figure 7.4, a surface with a positive mean curvature is locally convex, while a surface with a negative mean curvature is locally concave. The connectivity of a surface can be compared with a mountain landscape with the lakes and rivers through it. If the landscape is connected with convex curvatures, than the fluid can flow in the convex rivers through the whole landscape. In contrast, If the landscape is connected with concave curvatures, than the fluid will be captured within these lakes and is not possible to flow over the concave mountains, which impede the flow through the whole landscape. These distinct surface shapes can be used to predict the behavior of fluid flow.

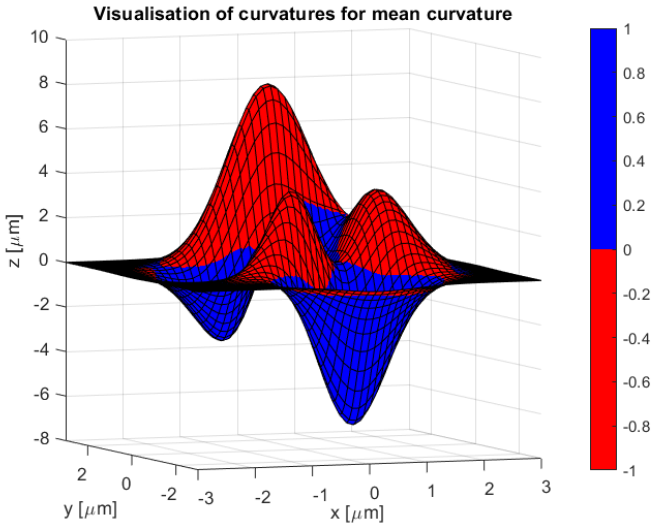

Figure 7.4: Mean curvature

In Figure 7.5 the mean curvature network of a reference glass bead and a modified glass bead treated with acid are presented. The image of the modified glass bead illustrates the presence of negative mean curvatures on the surface of the glass bead, which results in the formation of a connected network of boundaries for fluid flow. As can be observed, these boundaries create a complex network, which impede the flow over the surface. The fluid will stay within these boundaries and is unable to flow freely over the surface. The negative mean curvatures on the surface of the glass bead create a resistance to fluid flow, which leads to a decrease in the rate of fluid displacement.

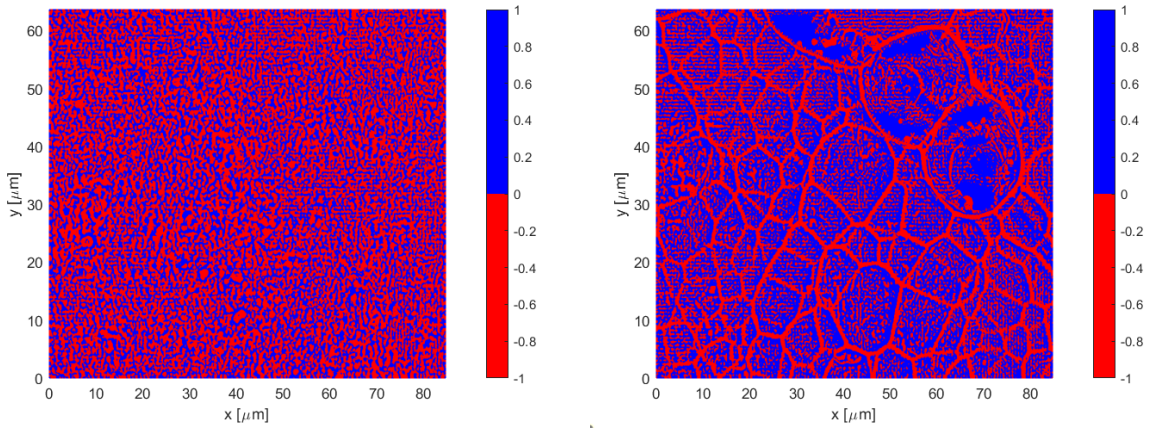

(a) reference glassbead

(b) modified glassbead

Figure 7.5: Mean curvatures glass

In Figure 7.6 the mean curvature network of a reference stainless steel sphere and a modified stainless steel sphere treated with acid are presented. The reference image depicts mean curvatures that are stretched in one direction across the plane. The observed stretched structure may be attributed to the presence of a face-centered cubic (FCC) crystal structure. Conversely, in the modified image, the stretched structure is no longer present and a more circular, disordered structure is observed. More similar with the reference structure of the glass beads. The stretched structure of the reference stainless steel sphere may result in a preferential flow direction for fluid, parallel to the stretched mean curvatures.

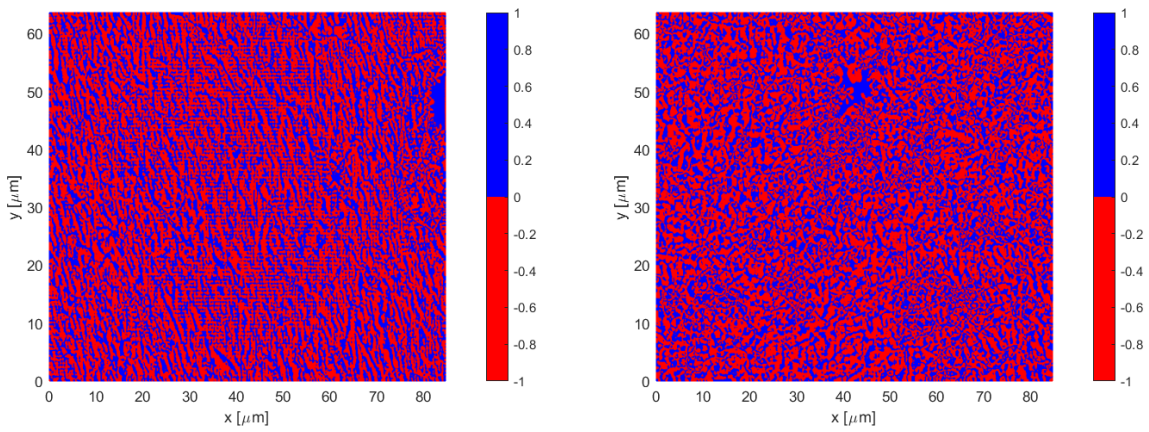

(a) reference stainless steel

(b) modified stainless steel

Figure 7.6: Mean curvatures stainless steel

7.3 Surface profile

In order to ensure the reliability of the data presented in the box charts, multiple samples were measured for each box. Specifically, for every box in the box charts, six different samples were measured.

In order to accurately differentiate the roughness of a surface, roughness parameters are often employed. These parameters can be used to assess both local roughness, by examining shorter length scales, as well as global roughness, by considering longer length scales. Craters, as a physical feature on a surface, can vary greatly in terms of their size. Specifically, some craters have been observed to have a diameter of approximately 40 micrometers. In order to fully capture and assess the entirety of the crater, as well as its immediate surroundings, it has been determined that the largest length measurement that is utilized in determining the overall roughness of the surface is 60 micrometers. By using a range of roughness parameters, it is possible to gain a comprehensive understanding of the roughness of a given surface. In the study, all length measurements were obtained from the center of the confocal surface profilometer image. To capture various locations on the surface, the angle at which the measurements were taken was varied. It is important to note that the center point of each length measurement was consistently located at the center of the image. The image captured by the profilometer was obtained from the exact center of the spherical sample. So, every line measurement crosses the top-center of the sample, according to the confocal measurement. This methodology was employed to ensure consistency and accuracy in the data collection process.

7.3.1 Acid

In the top-view presented in Figure 7.7, it is evident that the acid exhibits distinct effects on the surfaces of glass and stainless steel. Specifically, the acid appears to create circular craters on the surface of the glass beads, while the surface of the stainless steel appears to be indistinguishable. Given these disparate results, it is necessary to investigate roughness parameters in order to properly categorize the roughness of the surfaces in question.

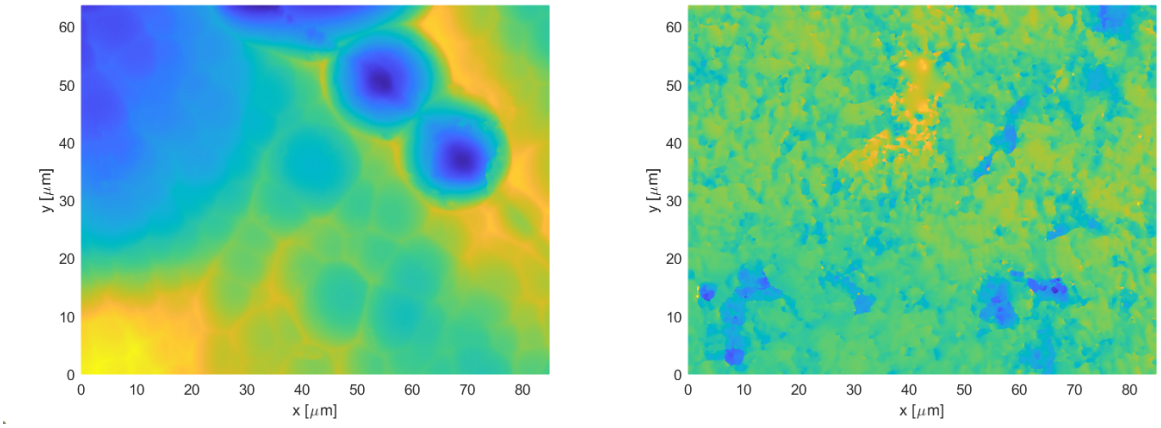

(a) glass (b) stainless steel

Figure 7.7: 2D top-view acid

The arithmetic average height has a significant impact on the wettability of the surface. With the increase of the pillar height, the droplet gradually transitions from a state of filling in the gap to a state of being held up by air.[11] The arithmetic average height of the surfaces of glass and stainless steel, as depicted in Figure Figure 7.8, exhibits notable differences. Specifically, for glass, the arithmetic average height increases significantly and the data exhibits a wider spread. In contrast, for stainless steel, the arithmetic average height more than double. however, the spread stays constant. This divergence in behavior can be attributed to the reaction of the acid with the surfaces of the materials, as seen in Figure Figure 7.7. It is worth noting that the values of the arithmetic average height are location-dependent, with significant differences observed just a few micrometers apart on the glass surface. This is indicative of the spread of the data. The increase in arithmetic average height on the glass surface can be explained by the presence of deep craters formed by the acid. The Peak-to-Valley and the arithmetic average height are closely related as can be seen. The plots are almost similar.

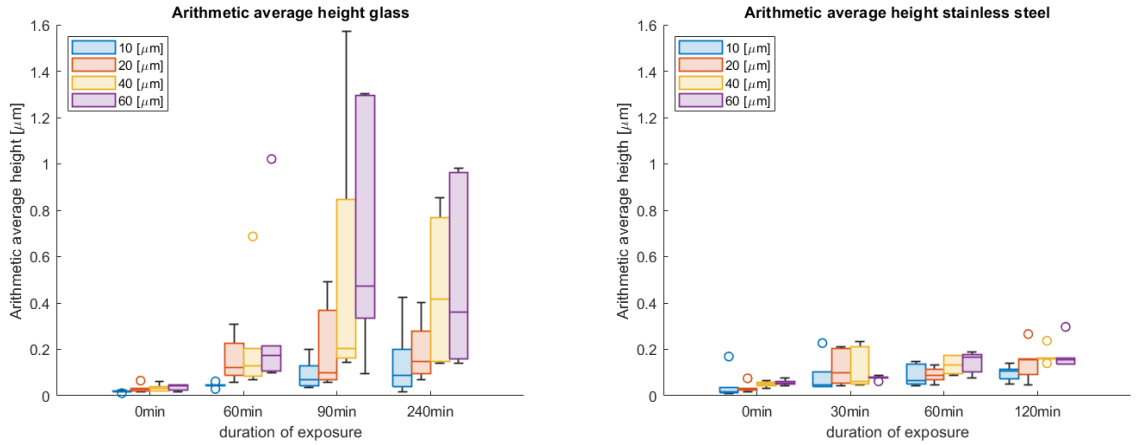

Figure 7.8: Arithmetic average height of different line lengths

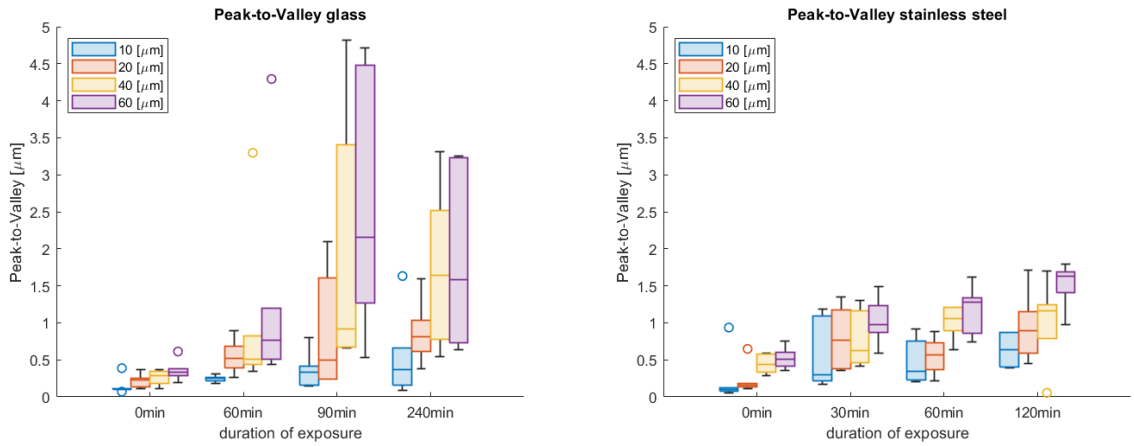

Figure 7.9: Peak-to-Valley for different line lengths

The mean spacing has a significant impact on the wettability of the surface.With the increase of the pillar spacing, the droplet contact angle gradually decreases. When the spacing is large enough, the droplet can enter the gap closest to the droplet and completely fill the gap.[11] The mean spacing for the glass beads appears to be inconsistent, with some seemingly anomalous values. However, these "zero-values" can be attributed to the fact that when a line length is taken within a crater, it will not rise above the mean line for a second time. Therefore, it is not possible to assign a value to this parameter in this instance. Similarly, the extremely high values for the larger line lengths can be explained by the fact that the borders of the crater fall within the line length, causing the profile to rise above the mean line twice. In contrast, the mean spacing for the stainless steel appears to be more consistent, with a spiky profile and relatively stable spacing between the spikes.

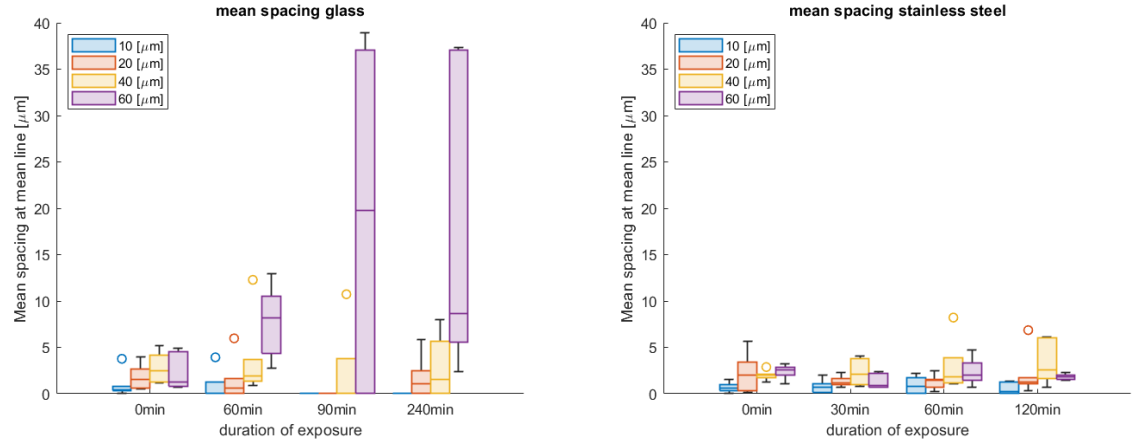

Figure 7.10: Mean spacing at mean line for different line lengths

The peak count, a metric used to quantify the number of peaks present in a given measurement line, is closely related to the mean spacing of those peaks. It is important to note that without a second pass through the mean line, it is not possible to accurately identify peaks in the measurement line. An interesting observation is that the peak count exhibits a wide spread of values, even in unmodified samples. In contrast, other parameters typically show minimal spread in unmodified data.

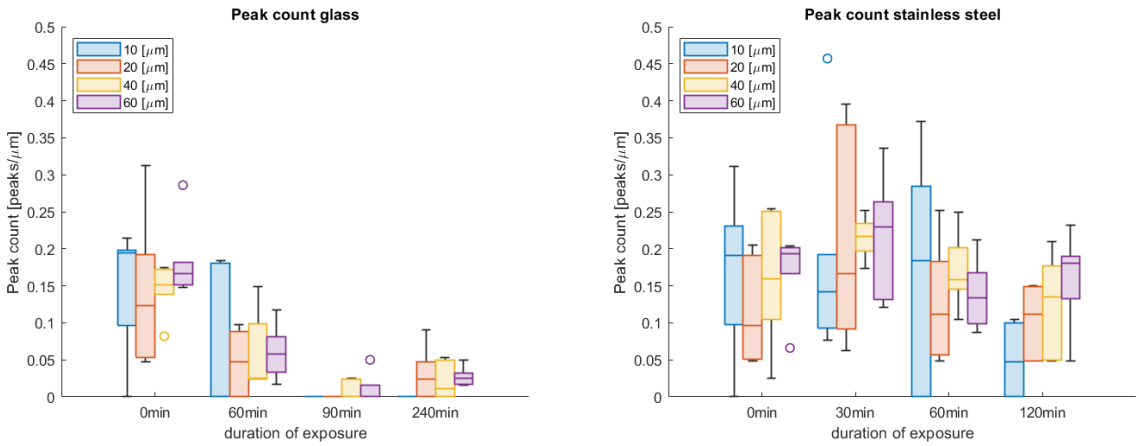

Figure 7.11: Peak count for different line lengths

The mean slope of the glass surface appears to remain consistent over time of exposure, with little variation in the spread of the data. This indicates that the slope of the surface profile does not significantly change during the exposure period. The mean slope of the stainless steel samples appears to more than double over time. This significant change in the slope of the surface profile may lead to a corresponding change in the fluid flow characteristics of the material.

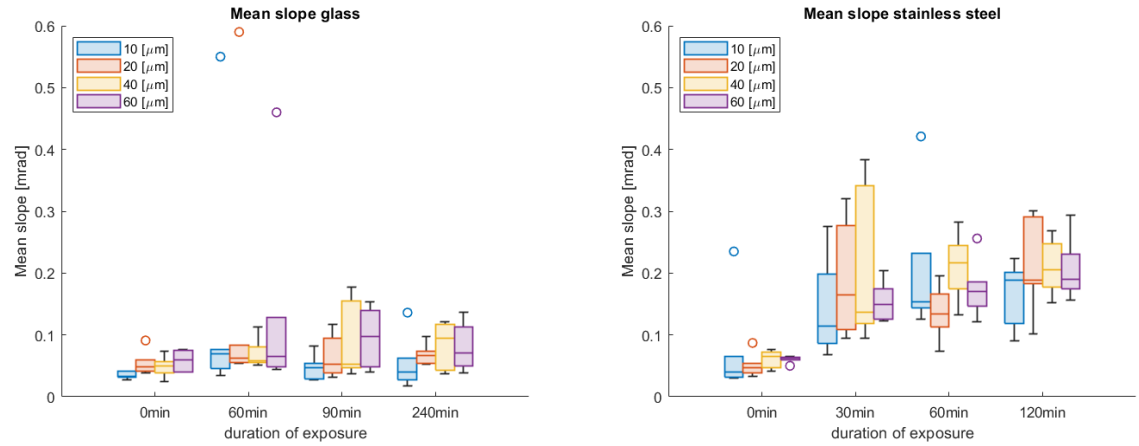

Figure 7.12: Mean slope for different line lengths

7.3.2 Sandpaper

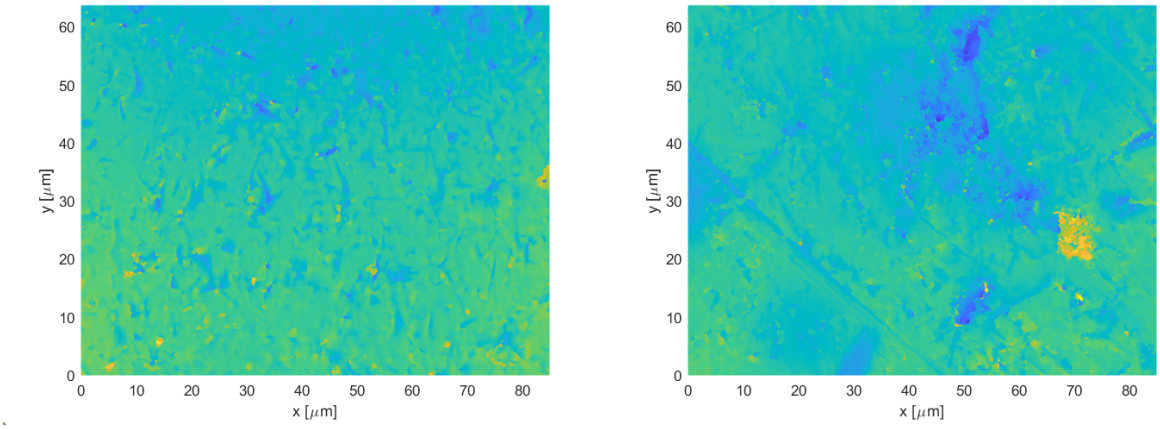

(a) glass (b) stainless steel

Figure 7.13: 2D top-view sandpaper

The amplitude parameters give an expected result for both glass and stainless steel. As can be seen in Figure 7.14 and Figure 7.15 the magnitude of both parameters increases, when the grain size increases. The other parameters will not be discussed in further detail. However, the graphs are shown in the appendix.

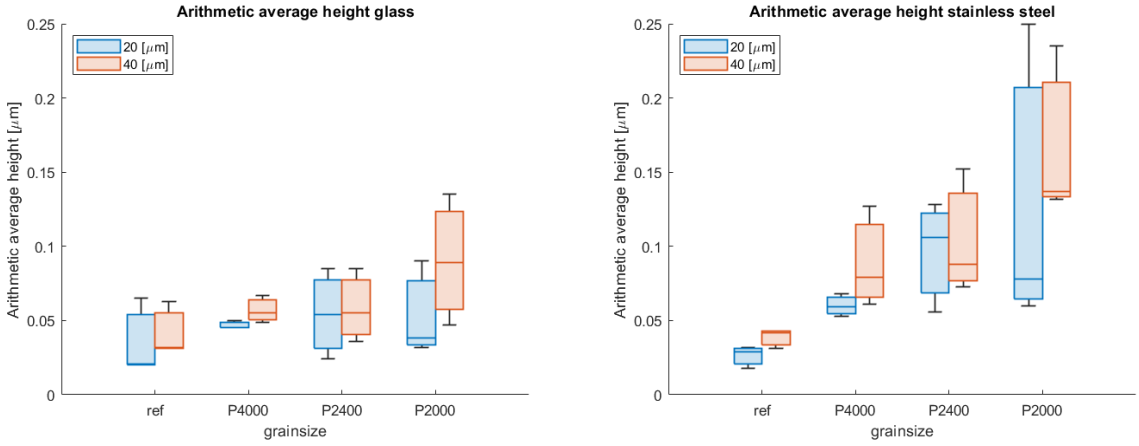

Figure 7.14: Arithmetic average height of different line lengths

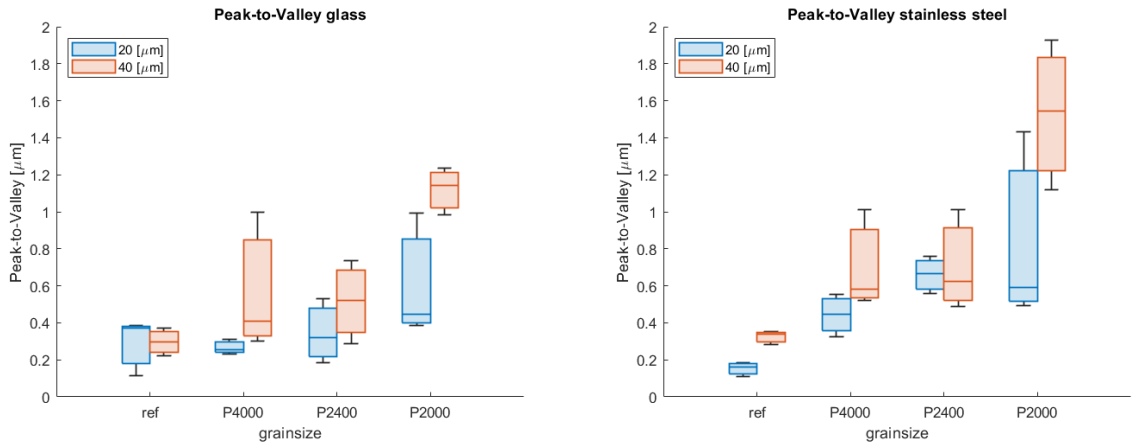

Figure 7.15: Peak-to-Valley for different line lengths

7.4 Roughness parameters over measured area

The software utilized in the analysis of the data was able to provide a comprehensive characterization of the measured surface area. However, only for three roughness parameters. By implementing this approach, a more global understanding of the sample's properties was obtained. Furthermore, in order to increase the precision of the data, each data point presented in the figures is an average of four measured areas. This method of averaging multiple data points improves the accuracy of the results, by reducing the effects of any local variations in the sample.

An analysis of the amplitude parameters was performed and it was observed that there was a significant increase in the amplitude for glass after the first hour of exposure to the acid. However, after the first hour a stabilization of the amplitude was observed. On the other hand, when analyzing the amplitude parameters of stainless steel spheres, it was observed that the increase was not as pronounced as in glass. Additionally, the amplitude was found to increase over time, indicating that it does not appear to reach a constant value within the measured exposure time. This suggests that the rate of etching for stainless steel spheres is slower than for glass, and that the amplitude continues to increase as the exposure time increases. This statement can be argued, because the exposure times are not similar.

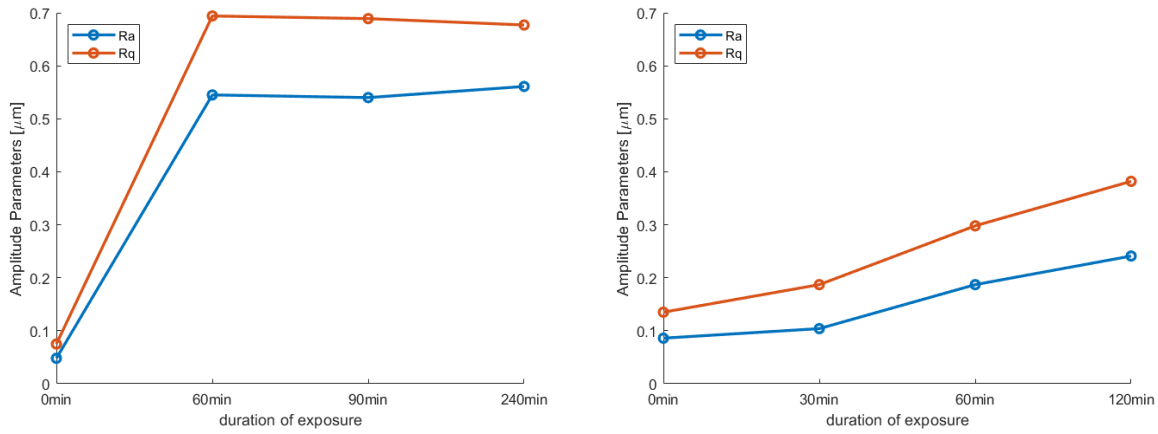

(a) glass

(b) stainless steel

Figure 7.16: Average amplitude parameters

An analysis of the hybrid parameter was conducted for glass and stainless steel. In the case of glass, it was observed that the slope stays constant over time. Despite the creation of these craters. The creation of these craters does not have any influence on the overall slope of the surface roughness. When analyzing the hybrid parameter for stainless steel, it was found that the slope increases over time. This result shows that the acid has a significant influence on the slope of the surface roughness.

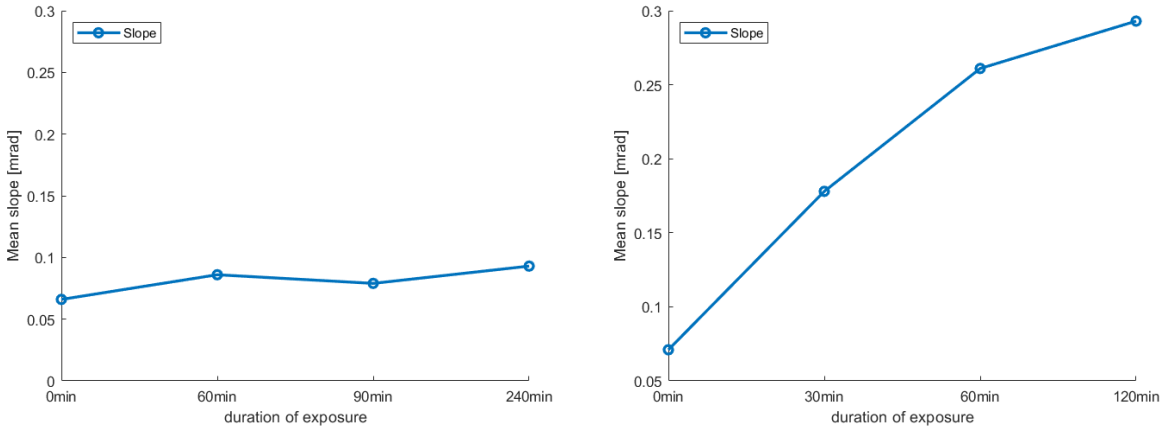

(a) glass

(b) stainless steel

Figure 7.17: Hybrid parameter

8 Discussion

In the following section, the correlation of the results will be discussed.

8.1 Influence of the acid on glass

Hydrofluoric acid is an etchant that is commonly used in the glass industry. This is achieved by dissolving the silica, which constitutes the majority of the glass composition. The acid selectively dissolves the surface of the glass, resulting in the formation of small craters with a circular shape. This symmetrical etching pattern is a result of the acid's chemical properties, which allow for the circular craters on the glass surface. However, it is important to note that the size and shape of the craters created by HF acid can be influenced by the duration of exposure to the acid. In Figure 8.1 the chemical reaction is shown:

Glass

$$SiO_2(s) + 4HF(l) \rightarrow SiF_4(g) + 2H_2O(l)$$

$$SiF_4 + 2HF \rightarrow H_2SiF_6(aq)$$

$$SiO_2(s) + 6HF(l) \rightarrow H_2SiF_6(aq) + 2H_2O(l).$$

Figure 8.1: Chemical reaction glass and HF[19]

An analysis on the increase in surface area reveals that the surface area remains constant over time. However, when examining the roughness parameters, it is observed that the amplitude parameters exhibit an increase. While mentioned in the introduction, surface roughness creates additional surface area. It is found that the surface roughness does not create additional surface area for glass. The roughness parameters also show a wider spread in the data after duration of exposure to the acid. This shows that the etching with acid does not give a homogeneous effect on the surface of glass.

An analysis on the connectivity of the surface reveals that a network of boundaries is created on the surface of glass. These boundaries will impede the flow and eventually result in a 'break off'. In Figure 8.2 the 'break off' is depicted. As can be seen, the red fluid is trapped in one of the craters by the black solid and the blue fluid.

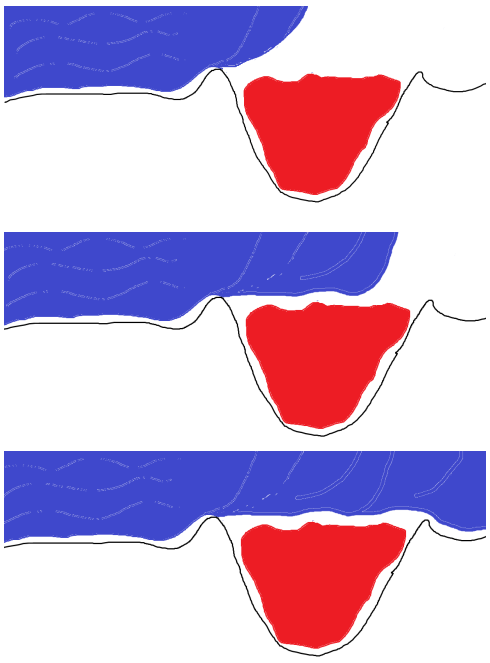

Figure 8.2: Break off

8.2 Influence of the acid on stainless steel

An analysis on the increase in surface area reveals that the surface area increases significantly. The increase after 120min of exposure to the acid is around 18 percent. This can be explained by the increase of some roughness parameters. As mentioned before, surface roughness creates additional surface area. The spreading of the data is far less relative to that of glass. The mean curvatures on the surface are chaotic and the surface can not be quantified as connective.

9 Conclusion

The goal is to quantify the surface roughness with several roughness parameters for different methods, to finally creating a 3D-model with a controlled surface roughness.

The use of glass etching as a method to simulate natural porous media has been found to be inadequate due to its lack of homogeneity. As demonstrated in the results, the roughness parameters of the etched glass exhibit a wide spread after a given exposure time. In order to achieve a realistic simulation of porous media, it is essential that the data is consistent.

Additionally, the acid used in the glass etching process creates distinct boundaries over the surface, resulting in captured fluid within these regions rather than a flow through the entire pore network. This deviation from the behavior of natural porous media further highlights the limitations of glass etching as a method for simulating porous media.

The use of stainless steel etching as a method to simulate natural porous media has been found more preferable. The increase of surface area and the roughness parameters give a predictable trend over exposure time. The data exhibit a compact spread, which is preferable for a realistic simulation of porous media.

The distribution of the mean curvatures on the other hand is chaotic and unpredictable. Which makes it hard to quantify the connectivity of the surface.

References

[1] M. J. Blunt, *MULTIPHASE FLOW IN PERMEABLE MEDIA A Pore-Scale Perspective*, 2017.

[2] zeroemissionplatform, "Safe Storage: Closing the carbon loop - CO2 Capture and Storage," 2010. [Online]. Available: https://www.youtube.com/watch?v=GglSLuWP5cM

[3] W. Lei, Q. Li, H. E. Yang, T. J. Wu, J. Wei, and M. Wang, "Preferential flow control in heterogeneous porous media by concentration-manipulated rheology of microgel particle suspension," *Journal of Petroleum Science and Engineering*, vol. 212, p. 110275, 5 2022.

[4] S. J. Park and M. K. Seo, "Solid-Liquid Interface," *Interface Science and Technology*, vol. 18, pp. 147–252, 1 2011.

[5] M. C. Alberto Giacomello, Simone Meloni and C. M. Casciola, "Cassie–Baxter and Wenzel States on a Nanostructured Surface: Phase Diagram, Metastabilities, and Transition Mechanism by Atomistic Free Energy Calculations," 6 2012. [Online]. Available: https://pubs.acs.org/doi/10.1021/la3018453

[6] M. A. E. N. R. R. A. S. S. Izman, Mohammed Rafiq Abdul-Kadir and M. Hassan, "Surface Modification Techniques for Biomedical Grade of Titanium Alloys: Oxidation, Carburization and Ion Implantation Processes," 3 2012. [Online]. Available: https://www.intechopen.com/chapters/32764

[7] Dongfang Yang and Alexis Laforgue, "Laser Surface Roughening of Aluminum Foils for Supercapacitor Current Collectors," 2019. [Online]. Available: https://iopscience.iop.org/article/10.1149/2.0601912jes/pdf

[8] Mike Klein, "Applications surface roughness," 10 2020. [Online]. Available: https://dryfinish.wordpress.com/2020/10/15/why-is-surface-roughness-so-important-in-manufacturing/

[9] E. S. Gadelmawla, M. M. Koura, T. M. Maksoud, I. M. Elewa, and H. H. Soliman, "Roughness parameters," *Journal of Materials Processing Technology*, vol. 123, no. 1, pp. 133–145, 4 2002.

[10] M. Kadivar, D. Tormey, and G. McGranaghan, "A review on turbulent flow over rough surfaces: Fundamentals and theories," *International Journal of Thermofluids*, vol. 10, p. 100077, 5 2021.

[11] B. Yin, X. Xie, S. Xu, H. Jia, S. Yang, and F. Dong, "Effect of pillared surfaces with different shape parameters on droplet wettability via Lattice Boltzmann method," *Colloids and Surfaces A: Physicochemical and Engineering Aspects*, vol. 615, p. 126259, 4 2021.

[12] Bruker Nano GmbH, "NanoWizard ® Series User Manual," Tech. Rep., 2021.

[13] NanoAndMore GMBH, "What is Atomic Force Microscopy (AFM)," 2019. [Online]. Available: https://www.nanoandmore.com/what-is-atomic-force-microscopy?gclid=CjwKCAiAoL6eBhA3EiwAXDom5uYRfL9s9-2yv0iyLCkyiuWS378q04JMuphLg8xcFETOK3mspPeGdRoCj4wQAvD_BwE

[14] JPK instruments, "jpk-tech-quantitative-imaging," *JPK instruments*, 2021.

[15] 'Sensofar Metrology', "Confocal principle," 2009. [Online]. Available: https://www.sensofar.com/metrology/technology/measuring-principles/confocal/

[16] Mike Yi, "Box plots," 2021. [Online]. Available: https://doi.org/10.1021/la3018453

[17] GeeksforGeeks, "Imperfection in Solids - GeeksforGeeks," 2022. [Online]. Available: https://www.geeksforgeeks.org/imperfection-in-solids/

[18] M. Deserno, "Notes on Differential Geometry with special emphasis on surfaces in R 3," Tech. Rep., 2004.

[19] toppr answr, "Glass reacts with HF," 2022. [Online]. Available: https://www.toppr.com/ask/en-ar/question/glass-reacts-with-hf-to-produce/

10 Appendix

10.1 roughness parameters sandpaper

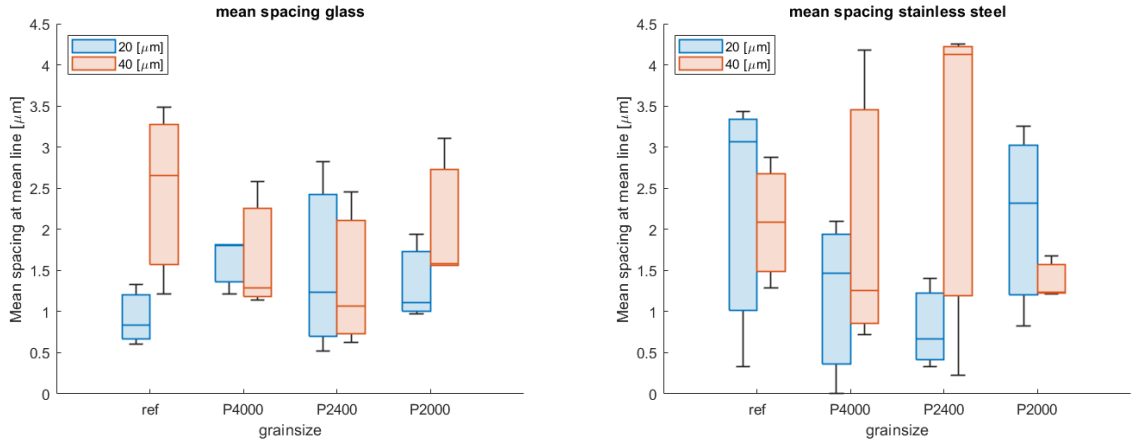

Figure 10.1: Mean spacing at mean line for different line lengths

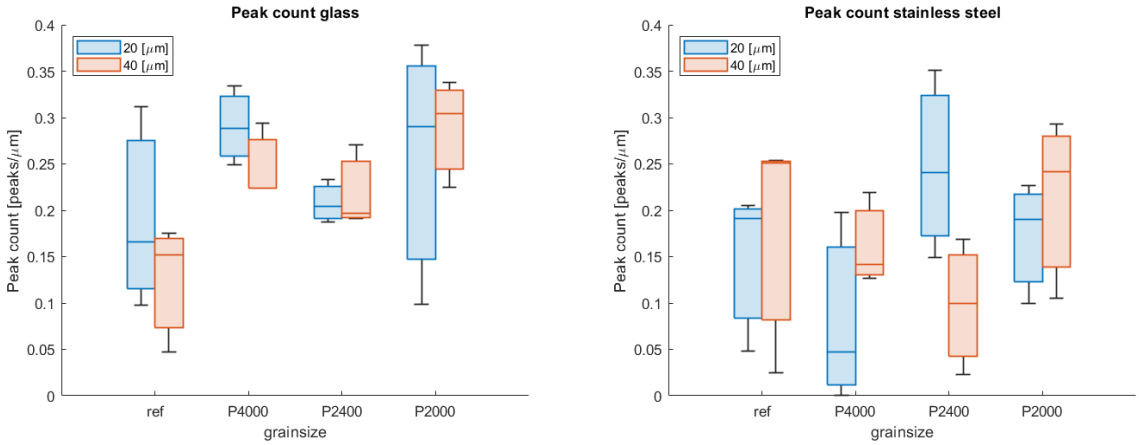

Figure 10.2: Peak count for different line lengths

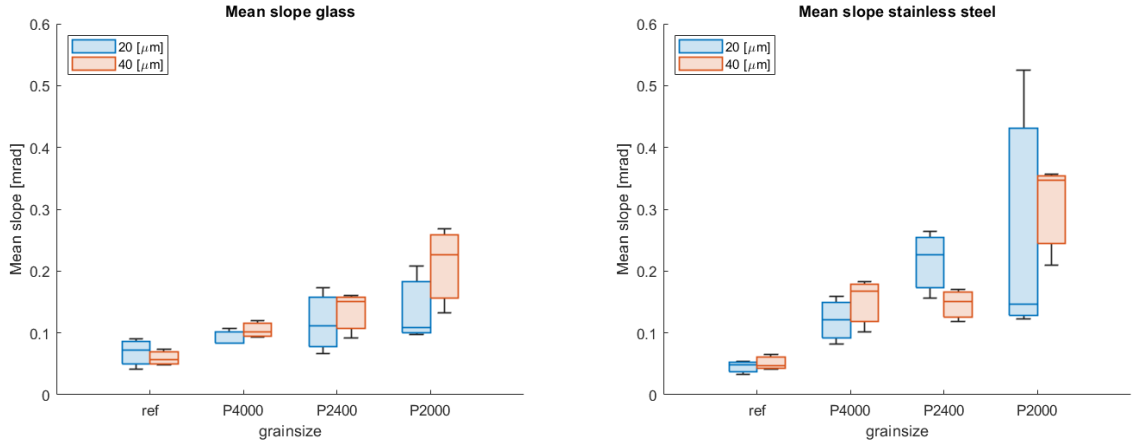

Figure 10.3: Mean slope for different line lengths

10.2 Roughness parameters etched glass different objectives

Reference 1	Amplitude			Spacing		Hybrid	
	Ra [um]	Rq [um]	PV [um]	Sm [um]	Pc [peaks/mm]	Δa [mrad]	Δq [mrad]
Glass zoom 20x	0.357	0.470	3.391	5.911	51.77	0.169	0.255
Glass zoom 50x	0.113	0.127	0.550	18.07	27.45	0.024	0.033
Glass zoom 150x	0.066	0.103	0.714	4.577	153.0	0.086	0.129

Reference 2	Amplitude			Spacing		Hybrid	
	Ra [um]	Rq [um]	PV [um]	Sm [um]	Pc [peaks/mm]	Δa [mrad]	Δq [mrad]
Glass zoom 20x	0.309	0.412	3.457	8.636	58.04	0.139	0.228
Glass zoom 50x	0.108	0.129	0.610	17.79	27.45	0.022	0.036
Glass zoom 150x	0.035	0.048	0.467	2.528	164.8	0.060	0.121

Reference 3	Amplitude			Spacing		Hybrid	
	Ra [um]	Rq [um]	PV [um]	Sm [um]	Pc [peaks/mm]	Δa [mrad]	Δq [mrad]
Glass zoom 20x	0.412	0.506	2.945	7.081	50.20	0.172	0.251
Glass zoom 50x	0.125	0.159	0.837	11.05	54.91	0.032	0.054
Glass zoom 150x	0.040	0.059	0.602	1.395	211.9	0.049	0.092

60min 1	Amplitude			Spacing		Hybrid	
	Ra [um]	Rq [um]	PV [um]	Sm [um]	Pc [peaks/mm]	Δa [mrad]	Δq [mrad]
Glass zoom 20x	1.014	1.988	51.88	9.742	29.81	0.407	2.083
Glass zoom 50x	0.639	0.858	3.539	44.60	11.77	0.058	0.095
Glass zoom 150x	0.817	0.958	3.226	34.29	11.77	0.104	0.161

60min 2	Amplitude			Spacing		Hybrid	
	Ra [um]	Rq [um]	PV [um]	Sm [um]	Pc [peaks/mm]	Δa [mrad]	Δq [mrad]
Glass zoom 20x	0.848	3.030	62.92	7.710	59.61	0.512	3.133
Glass zoom 50x	0.754	0.858	3.022	50.63	7.844	0.055	0.098
Glass zoom 150x	0.284	0.340	1.175	8.848	11.77	0.067	0.110

60min 3	Amplitude			Spacing		Hybrid	
	Ra [um]	Rq [um]	PV [um]	Sm [um]	Pc [peaks/mm]	Δa [mrad]	Δq [mrad]
Glass zoom 20x	1.946	2.608	33.80	15.01	18.83	0.449	1.775
Glass zoom 50x	0.483	0.709	3.295	28.77	11.77	0.043	0.075
Glass zoom 150x	0.292	0.463	3.052	5.309	35.32	0.068	0.095

90min 1	Amplitude			Spacing		Hybrid	
	Ra [um]	Rq [um]	PV [um]	Sm [um]	Pc [peaks/mm]	Δa [mrad]	Δq [mrad]
Glass zoom 20x	1.963	2.570	24.40	15.86	14.12	0.192	0.376
Glass zoom 50x	1.250	1.446	5.329	50.80	11.77	0.099	0.126
Glass zoom 150x	1.079	1.319	4.815	28.09	11.77	0.128	0.171

90min 2	Amplitude			Spacing		Hybrid	
	Ra [um]	Rq [um]	PV [um]	Sm [um]	Pc [peaks/mm]	Δa [mrad]	Δq [mrad]
Glass zoom 20x	3.785	6.247	50.11	51.46	14.12	0.419	2.100
Glass zoom 50x	0.821	0.955	3.073	20.42	7.844	0.046	0.063
Glass zoom 150x	0.128	0.160	0.676	4.120	47.09	0.048	0.065

90min 3	Amplitude			Spacing		Hybrid	
	Ra [um]	Rq [um]	PV [um]	Sm [um]	Pc [peaks/mm]	Δa [mrad]	Δq [mrad]
Glass zoom 20x	1.806	2.323	21.65	31.26	14.12	0.250	1.005
Glass zoom 50x	1.142	1.630	6.093	51.63	7.844	0.071	0.119
Glass zoom 150x	0.282	0.351	1.439	13.71	23.55	0.064	0.107

240 min 1	Amplitude			Spacing		Hybrid	
	Ra [um]	Rq [um]	PV [um]	Sm [um]	Pc [peaks/mm]	Δa [mrad]	Δq [mrad]
Glass zoom 20x	9.262	11.54	68.23	59.66	12.55	0.739	2.633
Glass zoom 50x	0.736	0.920	3.399	127.8	3.922	0.072	0.107
Glass zoom 150x	0.395	0.442	1.475	16.37	11.77	0.104	0.153

240 min 2	Amplitude			Spacing		Hybrid	
	Ra [um]	Rq [um]	PV [um]	Sm [um]	Pc [peaks/mm]	Δa [mrad]	Δq [mrad]
Glass zoom 20x	7.160	10.58	93.52	49.33	10.98	1.177	5.172
Glass zoom 50x	0.514	0.624	3.883	113.2	3.922	0.065	0.207
Glass zoom 150x	0.174	0.213	0.802	18.62	35.32	0.041	0.059

240 min 3	Amplitude			Spacing		Hybrid	
	Ra [um]	Rq [um]	PV [um]	Sm [um]	Pc [peaks/mm]	Δa [mrad]	Δq [mrad]
Glass zoom 20x	4.698	6.386	43.91	37.60	15.69	0.736	2.700
Glass zoom 50x	0.859	1.043	4.011	140.8	3.922	0.064	0.118
Glass zoom 150x	0.290	0.421	2.347	6.525	11.77	0.065	0.090

10.3 Roughness parameters etched stainless steel different objectives

Reference 1	Amplitude			Spacing		Hybrid	
	Ra [um]	Rq [um]	PV [um]	Sm [um]	Pc [peaks/mm]	Δa [mrad]	Δq [mrad]
SS zoom 20x	0.320	0.414	3.710	10.67	56.48	0.145	0.264
SS zoom 50x	0.128	0.239	2.280	10.33	39.22	0.049	0.141
SS zoom 150x	0.064	0.078	0.585	2.094	164.8	0.056	0.102

Reference 2	Amplitude			Spacing		Hybrid	
	Ra [um]	Rq [um]	PV [um]	Sm [um]	Pc [peaks/mm]	Δa [mrad]	Δq [mrad]
SS zoom 20x	0.384	0.498	4.048	13.09	47.06	0.154	0.271
SS zoom 50x	0.057	0.071	0.482	7.023	50.99	0.030	0.044
SS zoom 150x	0.057	0.067	0.336	4.142	129.5	0.063	0.102

Reference 3	Amplitude			Spacing		Hybrid	
	Ra [um]	Rq [um]	PV [um]	Sm [um]	Pc [peaks/mm]	Δa [mrad]	Δq [mrad]
SS zoom 20x	0.424	0.534	5.719	10.18	58.04	0.175	0.308
SS zoom 50x	0.079	0.109	0.828	4.437	86.28	0.042	0.070
SS zoom 150x	0.062	0.076	0.330	1.671	106.0	0.058	0.079

30min 1	Amplitude			Spacing		Hybrid	
	Ra [um]	Rq [um]	PV [um]	Sm [um]	Pc [peaks/mm]	Δa [mrad]	Δq [mrad]
SS zoom 20x	0.365	0.460	3.029	10.64	61.18	0.166	0.243
SS zoom 50x	0.063	0.077	0.419	4.553	83.36	0.036	0.055
SS zoom 150x	0.059	0.098	0.990	1.229	211.9	0.117	0.333

30min 2	Amplitude			Spacing		Hybrid	
	Ra [um]	Rq [um]	PV [um]	Sm [um]	Pc [peaks/mm]	Δa [mrad]	Δq [mrad]
SS zoom 20x	0.424	0.524	3.912	10.05	56.48	0.194	0.300
SS zoom 50x	0.111	0.159	1.413	6.806	54.91	0.057	0.136
SS zoom 150x	0.112	0.154	0.965	4.116	164.8	0.181	0.442

30min 3	Amplitude			Spacing		Hybrid	
	Ra [um]	Rq [um]	PV [um]	Sm [um]	Pc [peaks/mm]	Δa [mrad]	Δq [mrad]
SS zoom 20x	0.458	0.614	4.240	8.943	64.32	0.197	0.282
SS zoom 50x	0.060	0.108	0.867	2.469	62.75	0.043	0.075
SS zoom 150x	0.074	0.129	0.933	3.779	211.9	0.145	0.305

60min 1	Amplitude			Spacing		Hybrid	
	Ra [um]	Rq [um]	PV [um]	Sm [um]	Pc [peaks/mm]	Δa [mrad]	Δq [mrad]
SS zoom 20x	0.425	0.538	3.654	8.521	70.59	0.207	0.298
SS zoom 50x	0.155	0.196	1.337	11.34	50.99	0.062	0.108
SS zoom 150x	0.215	0.306	2.367	1.700	223.7	0.445	1.145

60min 2	Amplitude			Spacing		Hybrid	
	Ra [um]	Rq [um]	PV [um]	Sm [um]	Pc [peaks/mm]	Δa [mrad]	Δq [mrad]
SS zoom 20x	0.428	0.542	3.363	5.522	76.87	0.213	0.297
SS zoom 50x	0.098	0.134	1.001	5.518	82.36	0.054	0.079
SS zoom 150x	0.104	0.137	1.422	2.151	235.5	0.191	0.586

60min 3	Amplitude			Spacing		Hybrid	
	Ra [um]	Rq [um]	PV [um]	Sm [um]	Pc [peaks/mm]	Δa [mrad]	Δq [mrad]
SS zoom 20x	0.428	0.531	3.707	9.752	62.75	0.230	0.332
SS zoom 50x	0.097	0.161	1.284	3.536	78.44	0.060	0.107
SS zoom 150x	0.115	0.164	1.348	1.067	164.8	0.213	0.533

120min 1	Amplitude			Spacing		Hybrid	
	Ra [um]	Rq [um]	PV [um]	Sm [um]	Pc [peaks/mm]	Δa [mrad]	Δq [mrad]
SS zoom 20x	0.407	0.534	4.275	7.522	75.30	0.215	0.309
SS zoom 50x	0.132	0.189	1.224	5.155	74.52	0.073	0.118
SS zoom 150x	0.185	0.269	2.205	3.325	200.1	0.320	0.715

120min 2	Amplitude			Spacing		Hybrid	
	Ra [um]	Rq [um]	PV [um]	Sm [um]	Pc [peaks/mm]	Δa [mrad]	Δq [mrad]
SS zoom 20x	0.380	0.492	4.298	7.329	73.73	0.218	0.321
SS zoom 50x	0.125	0.180	1.282	6.723	78.44	0.068	0.136
SS zoom 150x	0.259	0.413	2.756	1.301	200.1	0.332	0.781

120min 3	Amplitude			Spacing		Hybrid	
	Ra [um]	Rq [um]	PV [um]	Sm [um]	Pc [peaks/mm]	Δa [mrad]	Δq [mrad]
SS zoom 20x	0.465	0.581	4.212	11.67	50.20	0.187	0.275
SS zoom 50x	0.381	0.555	3.034	6.345	70.59	0.126	0.327
SS zoom 150x	0.170	0.219	1.165	1.612	264.8	0.212	0.376